https://dx.doi.org/10.1016/j.oceaneng.2020.107499

Experimental and 3D Numerical Investigation of Solitary Wave Forces on Coastal Bridges

Deming Zhu[1] and You Dong[2, *]

Abstract:

In this paper, solitary wave-induced vertical and horizontal forces on coastal bridges are investigated by laboratory experiments as well as computational fluid dynamics (CFD) analysis. The effects of different parameters (e.g., water depths, submergence depths and wave heights) on wave-induced force on a 1:30 scale bridge model are studied. Specifically, the models of deck with and without girders are tested to explore the effects of girders and trapped air on structural performance. It is demonstrated with the collected experimental data that girders can increase the wave loads acting on decks and the trapped air makes the structure more unstable. Additionally, a secondary impact may occur due to the bluff profile of girders. Subsequently, based on solitary wave theory and experimental data, a linear relationship is quantified between wave forces and wave steepness. Following the experiments, numerical analysis using both two-dimensional (2D) and three-dimensional (3D) models is conducted to assess vertical and horizontal forces. The comparisons between experimental study and numerical computation indicate that the 2D model can well assess most of the cases for deck without girders, but fails to simulate accurate results for deck with girders, indicating that 2D model cannot deal with complex interactions between wave and structure. The 3D model can obtain more accurate wave forces, and better capture the detailed characteristics of solitary wave forces. With the information presented in this work, it can aid the design and management of coastal structures under hurricane and tsunami effects.

Keywords: Coastal bridges; Solitary wave; Experiments; Numerical analysis; Wave forces; 3D model

[1] Research Assistant and Ph.D. student, The Hong Kong Polytechnic University, Department of Civil and Environmental Engineering, Hung Hom, Kowloon, Hong Kong, d.m.zhu@polyu.edu.hk.

[2] Assistant Professor of Structural Engineering, The Hong Kong Polytechnic University, Department of Civil and Environmental Engineering, Hung Hom, Kowloon, Hong Kong, you.dong@polyu.edu.hk. *Corresponding Author.

1. Introduction

Based on historical data, extreme waves caused by hurricanes and tsunamis could lead to significant damages to our coastal community. For instance, Hurricane Isabel (2003), struck North Carolina and Virginia coastline, resulting in 17 deaths and more than 3 billion dollars in damages. The Indonesia tsunami (2004) destroyed many structures along the coast, leading to approximately 1200 deaths. With respect to the coastal bridges, especially for the low-lying ones, they are vulnerable to the storm surge and wave induced forces and could result in severe damages and failure. Considering climate change, increasing sea level rise, and amplification of hazard intensity, it demonstrates an urgent need for deeper understanding on failure mechanisms of coastal bridges and preparing for future disasters (Dong and Frangopol 2017; Frangopol *et al*. 2017). Douglass *et al*. (2004), Robertson *et al*. (2007a), Padgett *et al.* (2008) and Okeil and Cai (2008) conducted studies on the damage assessment of coastal bridges during Hurricane Ivan and Hurricane Katrina, and accordingly, one of the major failure modes of bridges under extreme waves is the unseating of deck (Akiyama *et al*. 2012; Kosa 2011; Bricker and Nakayama 2014; Robertson *et al.* 2007b). The total wave force on bridge superstructure consists of hydrodynamic and hydrostatic forces caused by large waves, and the short-duration shock force caused by the trapped air between girders and deck (Xu *et al*. 2016a; Azadbakht *et al*. 2016; Hayatdavoodi *et al*. 2014; Hayatdavoodi and Ertekin 2016; Seiffert *et al.* 2014b). The combination of these forces can overcome the weight of the superstructure and leads to the connection failure, and thus, the bridge deck is unseated away from the substructure (Ataei and Padgett 2012). However, the way that the wave forces work is complicated and affected by many parameters including wavelength, period, wave height, celerity and frequency, as well as the structure profile (Fang *et al.* 2019b). In addition, the prototype scale wave forces could only be approximated in situations with no trapped air, or air fully trapped between girders (Seiffert *et al.* 2015), while which is highly complicated in real hazard. Therefore, it is important to conduct further research on wave effects and structural response under extreme hazards for better management of existing and future coastal bridges.

Due to the complexity of wave-structure interaction, laboratory experiment is always one of the most direct and effective methods to explore wave forces (Guo *et al.* 2016; Fang *et al.* 2019a; Huang *et al.* 2019b). Although there were some laboratory tests focusing on the wave forces on coastal platforms and harbor wharfs (French 1970; Lee and Lai 1987; Boccotti 1995; Huseby and

Grue 2000), few studies investigated the impact of wave loads on bridge decks. Crowley *et al*. (2018) and James *et al*. (2015) compared test data of wave loads on bridge decks with existing analytical method associated with coastal platforms. They concluded that the established method for platforms cannot be used for bridges. Bradner *et al*. (2011) conducted an experiment of a 1:5-scale bridge model to measure wave forces under regular and random waves, observing a second-order relationship between force and wave height. Cuomo *et al*. (2009) experimentally investigated the quasi-static wave force and impulsive force on the bridge, and proved the contribution of trapped air. McPherson (2008) conducted the experimental studies using a large-scale 3D wave basin and compared experimental data with analytical results using existing models. It was concluded that most used prediction equations cannot sufficiently predict the measured forces. Guo *et al.* (2015a) investigated wave forces acting on superstructure of coastal bridges under regular waves and the experimental results were deviated from the analytical results as well. This series of experiments laid the foundation for later research, and explained some qualitative relationships for such phenomenon. Due to the diversity of wave parameters and forms, although some data have been obtained, they fail to reach a precise conclusion of the relationship between induced force and wave parameters (Guo *et al.* 2015b). Therefore, more experimental studies are needed to investigate the structural performance under wave by considering different scenarios and to improve the accuracy and efficiency of the analytical estimation of wave inducted forces on the coastal bridges.

Because of the complexity and huge cost of the experiment, especially for large scale studies, numerical analysis is also well accepted and proved its effectiveness. Combination of experimental and numerical investigation is an effective method to explore the complex wave-structure interaction (Seiffert 2014). The two-dimensional (2D) numerical simulation has been widely used within the computation of wave loads on coastal bridges. Huang and Xiao (2009) used the 2D RANS equations along with k-ε turbulence model to analyze the wave force on bridge decks. The influence of submersion water depth on the total uplift wave force was analyzed by using a similar method on the Biloxi Bay bridge decks (Xiao *et al*. 2010). However, in some cases, the 2D model could not identify some critical issues within the numerical analysis process. For instance, Jin and Meng (2011) used the commercial CFD software to simulate the wave-bridge interaction of the I-10 bridge over Escambia Bay and found that there still exist some differences between their 2D computational results and the calculated ones. Seiffert *et al*. (2014a) simulated a range of model

water depths and tested the role of entrapped air by using a 2D model with the open source CFD software, OpenFOAM. However, the results are limited to the case where there is no lateral flow of air, and thus a more sufficient simulation (e.g., 3D model) or test is required. Xu *et al*. (2016b) conducted numerical research of solitary wave forces on bridge superstructure based on component level, and pointed out that the 2D numerical simulation may not fully capture some features of wave-induced forces. Simplification by using 2D model could lead to some errors, and the 3D model should be studied in order to better analyze the wave process (Bozorgnia and Lee 2012; Motley *et al*. 2015). Thus, with respect to the bridges with complex geometries and bluff profile, it is necessary to perform 3D numerical simulation to account for the complicated deck-wave interaction. Also, discussion and comparisons of the differences between 2D and 3D computational models should be conducted. All these relevant aspects are investigated in this paper. Additionally, the relevant analytical results from both 2D and 3D models are compared and verified by the experimental data.

This paper aims to investigate solitary wave loads on bridge superstructure by both experimental and numerical studies. Though the solitary wave loads on the bridge were investigated by some of previous studies (Huang *et al.* 2019a, b; Xu *et al.* 2017b), a systematic investigation incorporating both 3D numerical model and experimental study is still needed especially for the investigated T-type girder bridge. In this study, a series of experimental studies on a 1:30 scale bridge model is conducted. Different water depths, water surface elevations, and submergence cases are selected and tested for the deck with and without girders. Both horizontal and vertical forces are measured. The effects of these parameters on wave forces are discussed. Additionally, a linear relationship between wave force and wave steepness is observed, and an equation calculating wave-induced force acting on bridge superstructure is proposed based on these parameters. As for numerical studies, both 2D and 3D models are adopted in this study and the relevant results are compared with the data from experimental studies. The wave profiles obtained from experiment, 2D model and 3d model are compared and discussed. Furthermore, effects of the trapped air from irregular and complex shape of bridge superstructure are analyzed as well. The experimental investigation is presented in section 2. Numerical model establishment and validation are described in section 3. Comparison between experimental and numerical results are shown in section 4. Finally, conclusions are drawn, and further work is noted in section 5.

2. Experimental investigation

2.1. Experimental facilities and design

The wave load experiments were conducted in the irregular wave channel at the Hydraulics Laboratory of the Hong Kong Polytechnic University. The wave channel is 27 *m* long, 1.5 *m* wide, and 1.5 *m* deep, as shown in Fig. 1(b). A piston-type wavemaker is used to generate waves at one side of the wave channel. At the opposite side of the channel, a wave absorber is equipped to dissipate energy. Water surface elevation is measured using three capacitive wave height gauges. A multi-axis load cell is used to measure forces at *x* (same direction as the wave propagation), *y* (perpendicular to the wave propagation), and *z* (vertical to the ground) directions, respectively. Forces data are sampled at a frequency of 1000 *Hz*, which is sufficient for this experiment as the force events occur approximately within a 1~2 *s* window as shown in the Experiment Results section.

(a) 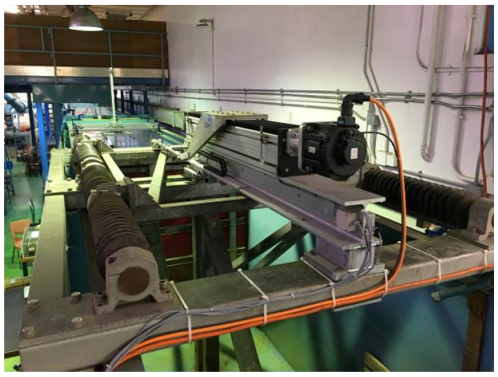 (b) 

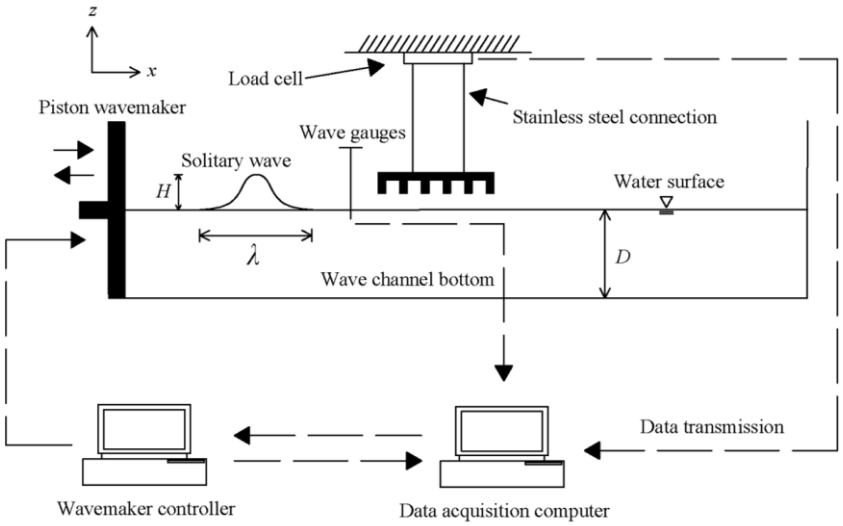

(c)

Fig. 1 (a) DHI piston wavemaker; (b) 27 m long wave channel; and (c) schematic diagram of experimental setups

The experiments were designed according to the Froude similarity model (open channel flow). A 1:30 scale model bridge is tested in the laboratory experiment. The prototype bridge is a typical simply supported bridge widely built in coastal regions. Due to years of service and increasing sea level rise, some of these bridges are under high risk from hurricane and tsunami. The detailed information and damage report of this type bridge under wave-induced force can be found in Douglass *et al.* (2004). The model is made of clear acrylic and attached to stainless steel bar, as shown in Fig. 2(a). The pulley on the left side of the model is used for calibration of the load cell in the horizontal direction, and was removed during the experiment. For better observation of wave-deck interaction, the side of the model is painted red. The bridge model of the deck without girders is shown in Fig. 2(b). The model of deck with girders is composed of a deck and six girders evenly distributed along the width of the deck, as presented in Fig. 2(c). The span length and width of the deck are 580 *mm* and 320 *mm* respectively and the thickness is 20 *mm*. All six girders have a height of 38 *mm* and a width of 20 *mm*. The four small round holes are used to connect the structure to the load cell by stainless steel bars. Waterproof measures are set around these holes to prevent the leakage of compressed air caused by the extreme waves. The bridge model is set at a distance of 8 *m* from the wave generator paddle. The clearance, which is calculated from the wave basin bottom to the bottom of the bridge deck (for both deck with and without girders), is set as 0.55 *m*, corresponding to a prototype size of 16.5 *m*.

A total of 176 cases were tested, 88 for the no girder cases and 88 for the girder cases. 11 different heights H ranging from 0.10 *m* to 0.20 *m* with an interval of 0.01 *m* were tested under 8 different depths D (0.48 *m*, 0.50 *m*, 0.52 *m*, 0.54 *m*, 0.56 *m*, 0.58 *m*, 0.60 *m*, and 0.62 *m*). These cases cover a range of realistic prototype wave heights from 2.4 - 6.6 *m* and water levels from 14.4 - 18.6 *m*. Fully submerged conditions (D = 0.58 *m*, 0.60 *m* and 0.62 *m*) are also tested considering potential impact of climate change, increasing sea surface level, and hurricane-induced storm surge on the old bridges with small designed clearance.

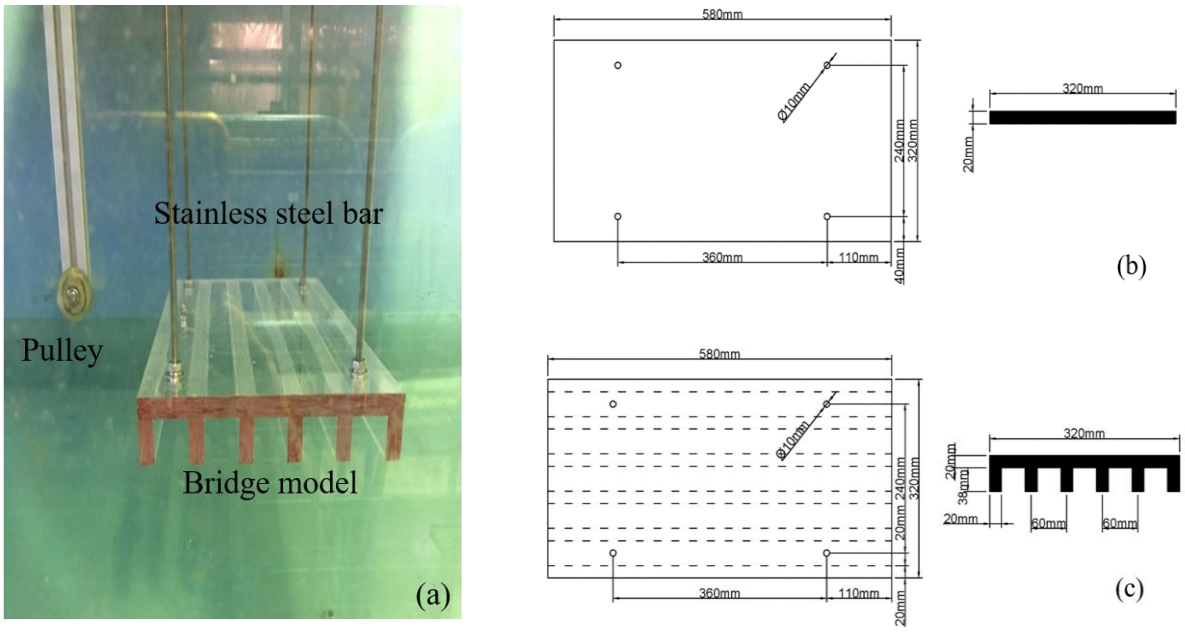

Fig. 2 (a) Photo of the experimental setup; plan view and cross section of (b) deck without girders; and (c) deck with girders

2.2. Wave generation method

Solitary waves were generated by using a piston-type wavemaker controlled by the software DHI Wave Synthesizer (Danish Hydraulic Institute). The control strategy of the paddle motion is based on the Boussinesq (1872) theory, which describes the wave profile and forms an exact solution of the Korteweg-de Vries (KdV) equation. The dimensional quantities of such wave theory are:

$$\eta(x,t) = H\,\mathrm{sech}^2\sqrt{\frac{3}{4}\frac{H}{D^3}}(x-ct) \tag{1}$$

where c=$\sqrt{\mathrm{g}(D+H)}$. In these formulas, η is the free surface elevation above still water level (SWL); t is time; H is wave height; D is water depth; and c is wave celerity.

The field inspection results of past natural hazards indicated that such huge wave forces acting on coastal bridges depended significantly on wave height and relative clearance between the bridge superstructure and SWL (Ataei and Padgett 2012). Wave height H and water depth D are therefore often used as intensity measures for coastal bridge performance assessment under

hurricanes/tsunami. The adopted Boyssinesq solitary wave has the unique property that the wave profile is defined by the wave height *H* and water depth *D*, which makes it suitable to simulate the wave within experimental and numerical studies (Goring 1978; Kennedy *et al.* 2000; Chen et al. 2000). Given more information and specific scenarios, other models (e.g., McCowan 1891, Laitone 1963) could also be used to generate solitary wave (Naheer 1977; French 1970).

Biesel and Suquet (1951) discussed the wave generation for a number of different wavemaker types, and developed the wave generation theory to prescribe the displacement-time history of the piston wavemaker. For the generation of long waves which propagate with constant form (i.e., solitary waves), the wave function can be expressed as:

$$f(\theta) = \operatorname{sech}^2 \theta \tag{2}$$

where $\theta = \kappa(ct - \xi)$; $\kappa = \sqrt{\frac{3}{4}\frac{H}{D^3}}$ and ξ is the displacement of the paddle. Thus, the displacement is

$$\xi(t) = \frac{H}{\kappa D} \tanh \kappa(ct - \xi) \tag{3}$$

Based on Eq. (2), the origin of displacement ξ and time *t* is under the wave crest. In addition, the wave function f tends to be 0 as θ goes to infinity, which means the intercepts of the characteristics associated with the leading and trailing edges of the wave t_0 occurs at $\pm\infty$. Thus, in order to meet the wave generating device design and practical purpose, the intercepts t_0 is defined with a precision of three significant figures and can be computed as (Goring 1978):

$$t_0 = \frac{\tanh^{-1}(0.999)}{\kappa c} = \frac{3.80}{\kappa c} \tag{4}$$

where t_0 is the time interval between wave crest and SWL. Accordingly, the approximate period of solitary waves *T* can be calculated as $2t_0$, and the effective wavelength λ can be obtained as the product of celerity and period.

Apart from the control signal of generating progressive wave, another term is utilized in control to avoid the disturb of generated waves. Although energy dissipation measures are set at

the end of the wave channel, as the waves hit the end of the channel, parts of the wave energy are still reflected and travel towards the wave generator. When the reflected wave reaches the wave generator, it is reflected. The result is a re-reflected wave travelling together with the directly generated solitary wave. In order to avoid the distortion of the re-reflected waves, an "absorption control" is applied by moving the paddle based on the surface elevation time series (Schäffer 2002). More detailed information about solitary wave generation and data acquisition method could be found in Goring (1978) and DHI Wave Synthesizer user guide, respectively.

2.3. Experimental results and discussion

2.3.1. Force time history

To obtain a better understanding of the characteristics of solitary wave loads, time histories of vertical and horizontal wave forces on the bridge models are analyzed and the wave forces are divided by the length of the model (0.58 *m*). It should be noted that in all the figures shown in the following sections, the origin of time *t* does not necessarily represent the starting point of the actual wave, but to better display the results.

Fig. 3 shows time series of the vertical and horizontal wave loads associated with the deck without girders under the case of $D = 0.5\ m$ and $H = 0.15\ m$. Under this circumstance, the deck model is elevated from the SWL to a certain height, and the wave height is large enough to hit and exceed the deck. For a better display of wave loads acting on the bridge model and distinguish the effects of structural vibration, a smoothed curve is fitted and shown as well as the measured data. As indicated, the solitary wave force is associated with an obvious peak and trough. Apart from the smoothed result expressed in dark lines, the extreme solitary wave also causes structure vibration to some extent. The vibration is clearly observed in horizontal wave force. When the wave crest first arrives at $t = 2\ s$, although the horizontal force does not reach the maximum value, it still causes rapid vibration of the structure. Since the wave hits only on seaward side of the bridge, structural vibration is asymmetric and positive forces (same direction of wave propagation) are larger than the negative forces (opposite direction of wave propagation). Such asymmetrical impact may also result in damage and failure of the connection between superstructure and substructure.

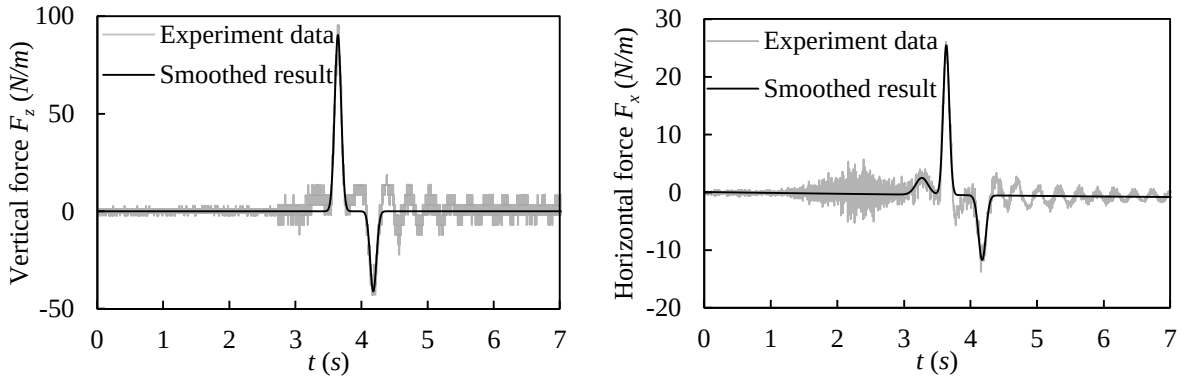

Fig. 3 Time histories of wave forces associated with the deck without girders given D = 0.5 m and H = 0.15 m

Fig. 4 presents the time history of wave forces on the girder deck with the same initial condition given D = 0.5 *m* and H = 0.15 *m*. Similarly, a smoothed curve is presented for better illustrative purpose. It is obvious that both vertical and horizontal wave forces are much larger than those of the no girders case. One difference is that the structural vibration occurs during the entire process of wave flow passing the structure. It can be concluded that girders not only result in larger forced area and wave loads, but also intensify the dynamic response and the instability of the structure.

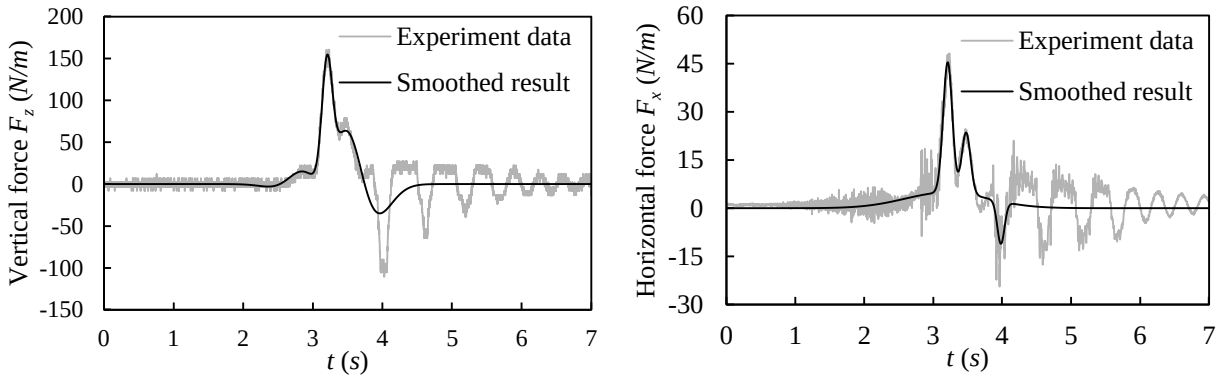

Fig. 4 Time histories of wave forces associated with the deck with girders given D = 0.5 *m* and H = 0.15 *m*

2.3.2. Secondary impact associated with girders

Another significant difference of the girder deck is that there is a secondary rise in the declining phase of the wave force. The force reaches its peak and drops, before reaching its second peak. The value of the second peak is about half of the maximum force, as shown in Fig. 5. In order to

further understand this characteristic, several cases are chosen and compared, including: (1) D = 0.5 m, H = 0.16 m; (2) D = 0.56 m, H = 0.16 m; and (3) D = 0.62 m, H = 0.16 m, as shown in Fig. 6. The three different initial water depths cover unsubmerged case, partially submerged case, and totally submerged case. It is obvious that as the initial water surface rises, the maximum force descends significantly, while the second peak changes little. The maximum uplift force is almost twice of the second peak in unsubmerged case, but they are almost the same in the partially submerged case and fully submerged case. Horizontal wave forces are presented as well. Forces with continuous fluctuation reflect the strong vibration of the structure, and values of two peaks get closer as the initial water depth increases. The measured secondary peak forces under these three water depths are shown in Fig. 6. Generally, it increases with larger wave height H. The unsubmerged case (D = 0.5 m) has the largest secondary impact, while these forces for partially submerged and totally submerged cases (e.g., D = 0.56 m and 0.62 m) are really close. Both the wave-structure dynamic interaction and the trapped air between the girders and deck could contribute to the secondary impact. The secondary impact force tends to stabilize with less trapped air (e.g., partially and totally submerged cases).

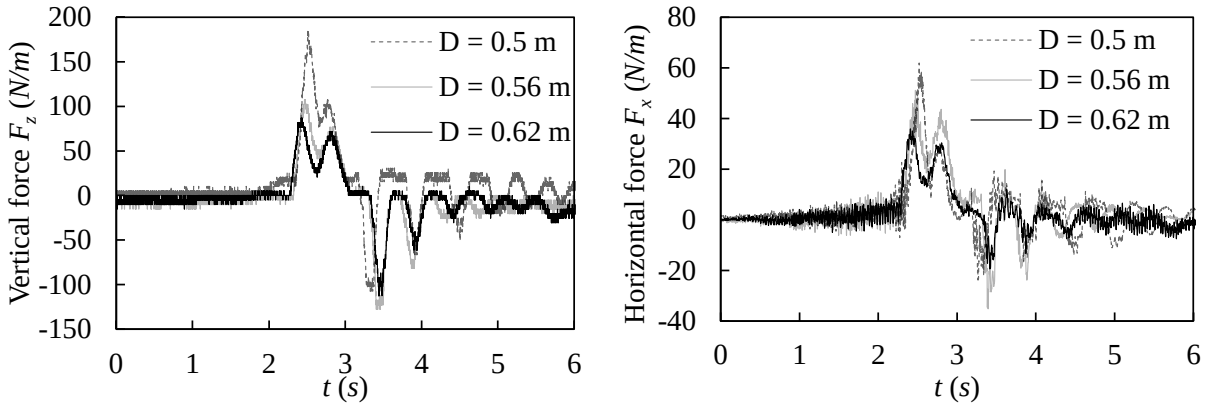

Fig. 5 Comparison of time histories of wave forces among the three cases: (1) D = 0.50 m, H = 0.16 m; (2) D = 0.56 m, H = 0.16 m; and (3) D = 0.62 m, H = 0.16 m.

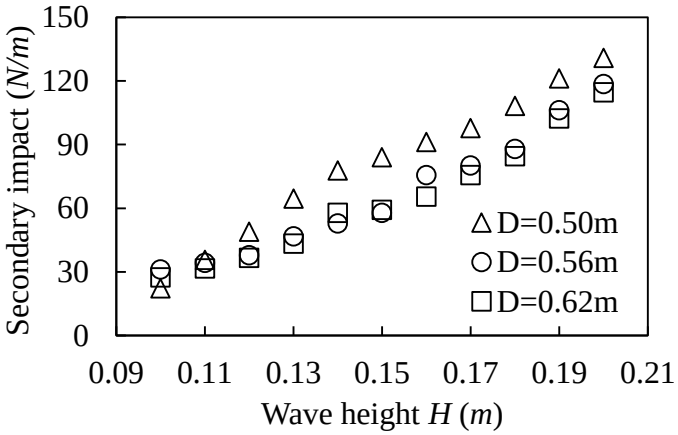

Fig. 6 Comparison of the uplift secondary impact when D = 0.50 *m*, 0.56 *m* and 0.62 *m*

2.3.3. Peak force

The experimental data of the deck without girders for the vertical uplift force F_u (maximum vertical force), vertical downward force F_d (absolute value of the minimum vertical force), horizontal positive force F_p (maximum horizontal force with the same direction of the wave), and horizontal negative force F_n (absolute value of the minimum horizontal force) under different water depths and wave heights are presented in Figs. 7, 8, 9, and 10, respectively.

Fig. 7(a) shows that uplift wave force increases nonlinearly with the wave height linearly increasing or the water depth linearly decreasing. The greatest uplift force occurs when the wave crests significantly exceed the top of the plate (H = 0.2 *m*) for all the water depths (i.e., D = 0.48, 0.50, 0.52, 0.54 *m*). The submerged case is shown in Fig. 7(b). As indicated, the uplift force increases linearly with the increase of the wave height. Horizontal positive forces (Fig. 8) keep an upwards trend with increasing H and decreasing D in unsubmerged cases, except for scenarios H < 0.15 *m*. As for submerged cases, larger positive forces are measured with larger wave heights. Overall, vertical uplift forces and horizontal positive forces are larger in unsubmerged cases than those in submerged cases under the same wave height H. This behavior may be related to the fact that the slamming force, which plays an important role in composing total wave forces, decreases or even disappears with a higher water depth.

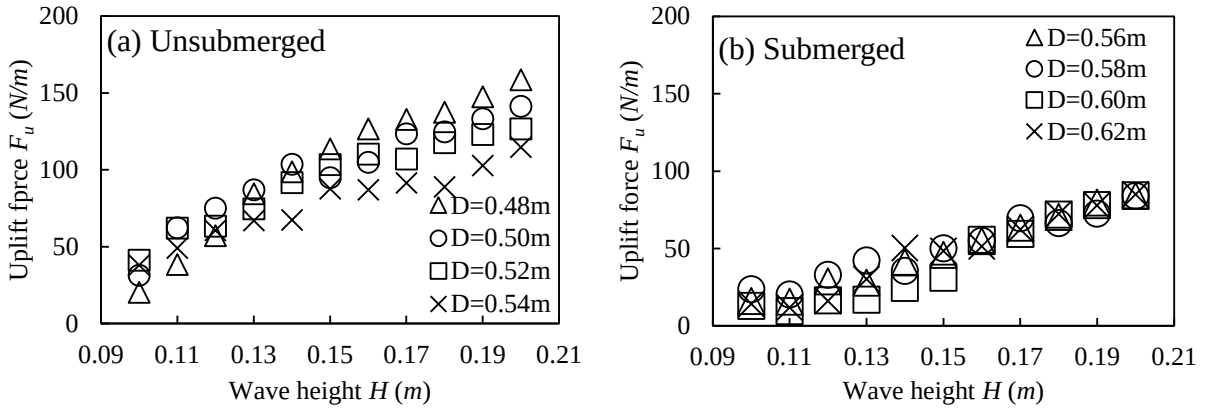

Fig. 6 Experimentally measured vertical uplift wave forces for deck without girders

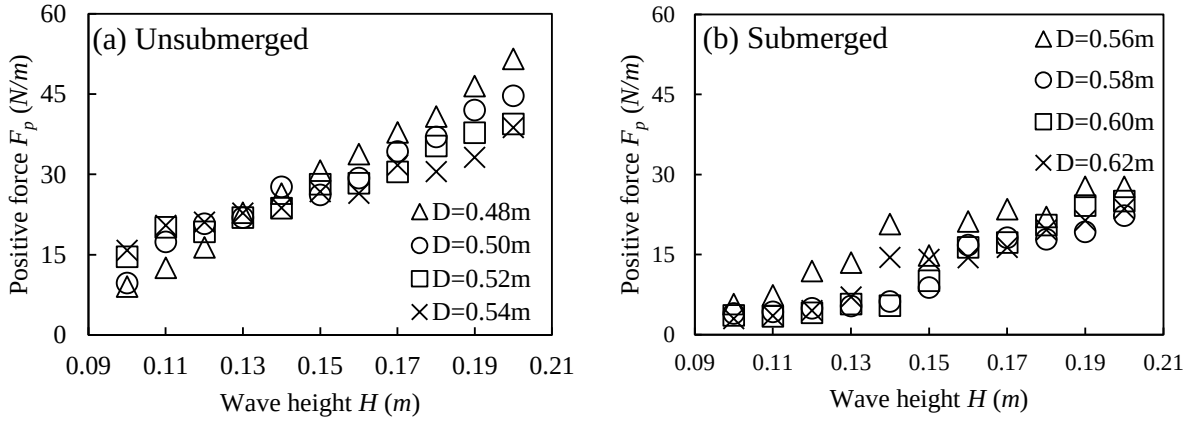

Fig. 8 Experimentally measured horizontal positive wave forces for deck without girders

The vertical downward forces are presented in Fig. 9. The downward forces show a totally different trends for unsubmerged cases, which have larger values when wave heights are larger (H = 0.19 and 0.20 m) or smaller (H = 0.10 and 0.11 m). The minimum value of F_d occurs at H = 0.15 m (given D = 0.48 and 0.54 m) and at H = 0.14 and 0.13 m (given D = 0.50 and 0.52 m). However, for the submerged cases, we only see larger downward forces under larger wave heights and smaller initial water depths, except for D = 0.62 m. Similarly, negative horizontal forces (Fig. 10) tend to decrease first and then increase with the increasing wave height except for D = 0.48 m. For all the wave heights, minimum values of F_n are measured when D = 0.54 m. For the submerged cases, although the negative forces still tend to increase with wave heights, they are not well ordered compared with vertical uplift forces. Such irregular change may result from the unstable energy dissipation and flow separation at the trailing edge of the wave.

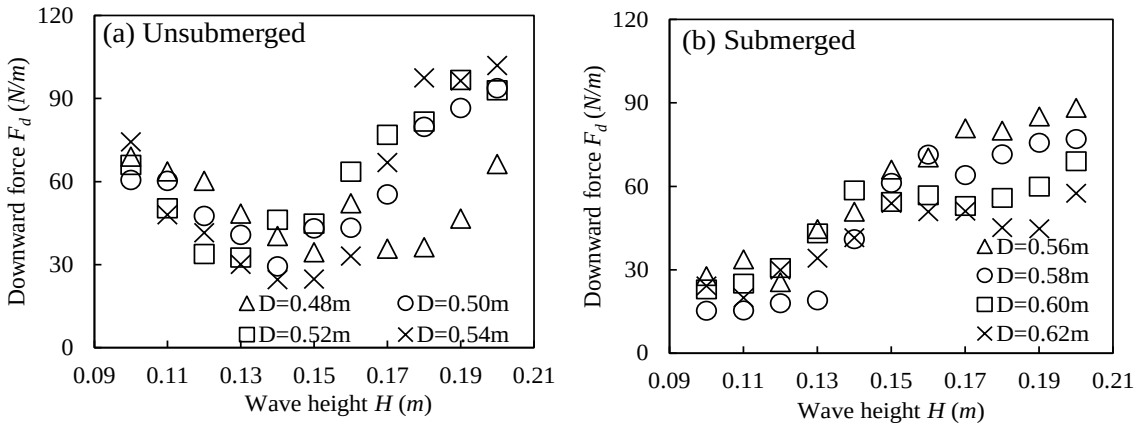

Fig. 9 Experimentally measured vertical downward wave forces for deck without girders

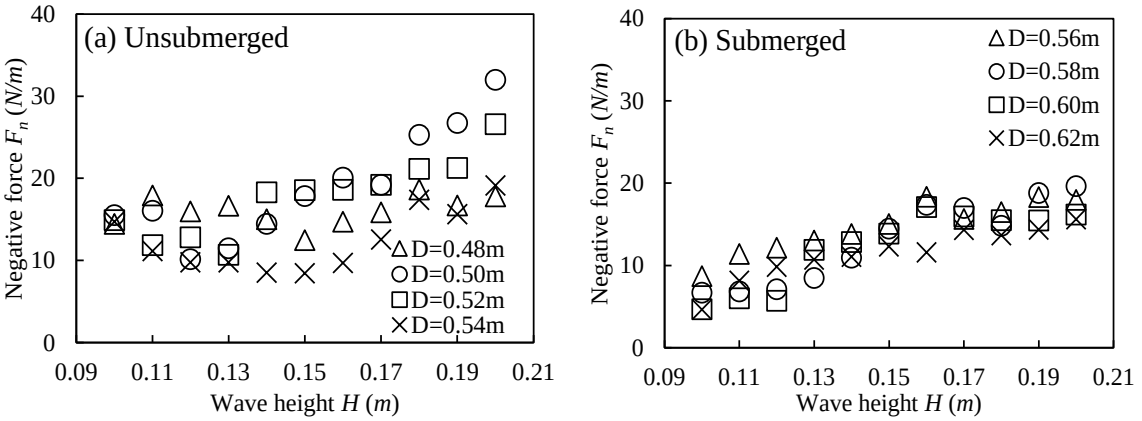

Fig. 10 Experimentally measured horizontal negative wave forces for deck without girders

Experimental data for the vertical uplift forces, horizontal positive forces, vertical downward forces and horizontal negative forces for the deck with girders under various water depths and wave heights are presented in Figs. 11, 12, 13, and 14, respectively. For unsubmerged cases, the whole bridge model is elevated from initial water surface, and waves are large enough to reach and exceed the bridge deck. For partially submerged cases, the initial water level reaches the bottom of girders but are lower than the top of the deck, so the quantity of trapped air decreases with the increasing initial water depth. For fully submerged cases, the initial water level is higher than the top of the deck. Overall, wave forces acting on the deck with girders are much larger than those on the deck without girders.

Similar trends are found in the vertical uplift forces and horizontal positive forces for the deck with girders. Both forces tend to increase with wave heights as shown in Figs. 10 and 11. For the

unsubmerged cases, positive forces for D = 0.48 m are larger than those for D = 0.50 m, while there exists no big difference in the uplift forces for these two scenarios. For partially submerged conditions, these forces increase with decreasing initial water depth for most wave heights, except for H = 0.13 and 0.15 m. These results may be related to the fact that quantity of trapped air decreases with increasing initial water depth, and thus leads to the decrease in the uplift force caused by the compressed air. For the fully submerged conditions, it is found that, vertical forces for D = 0.62 m are significantly less than the other two cases. With respect to the horizontal positive forces, there is again an increase in forces with smaller initial water depth, and the rate of increase in forces also increases.

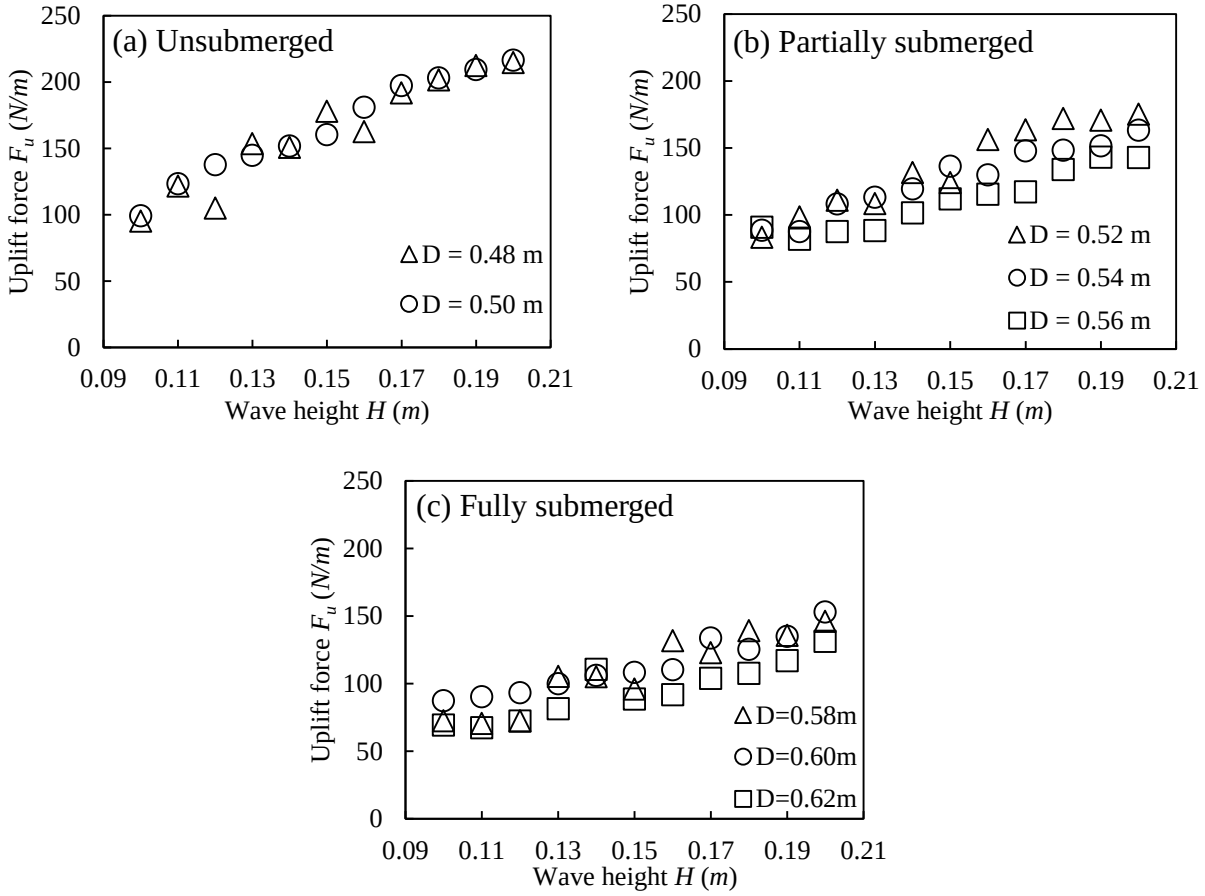

Fig. 11 Experimentally measured vertical uplift wave forces for the deck with girders

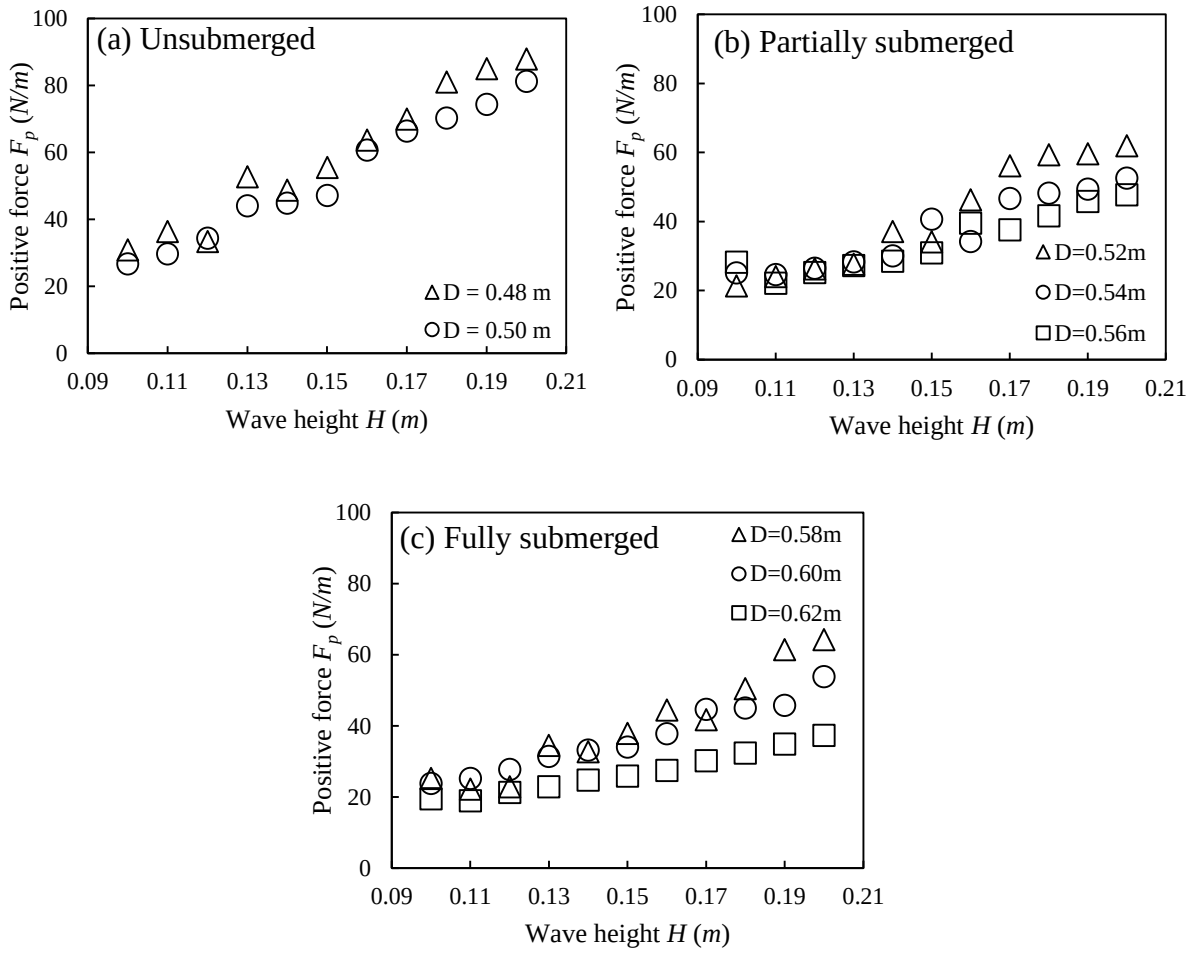

Fig. 12 Experimentally measured horizontal positive wave forces for the deck with girders

Fig. 13 shows the vertical downward forces. Different from those no girders cases, there is no obvious trough in the figure, but the forces increase in a nearly linear relationship with the increase of wave heights. For partially submerged cases and fully submerged cases, downward forces keep increasing with increasing initial water depth until the bridge is completely submerged. After that, the forces almost remain constant. For D = 0.48 and 0.50 m, negative horizontal forces remain stable with changes in wave heights. However, for partially submerged cases, that is D = 0.52, 0.54, and 0.56 m, there is again an increase in force with larger wave heights. Negative force for D = 0.56 m is the largest among the three cases when H < 0.17 m. For the case that H is greater than 0.17 m, the force is the smallest among the three. For fully submerged conditions, negative forces are affected profoundly by nonlinear effects, but do not change much as wave height varies.

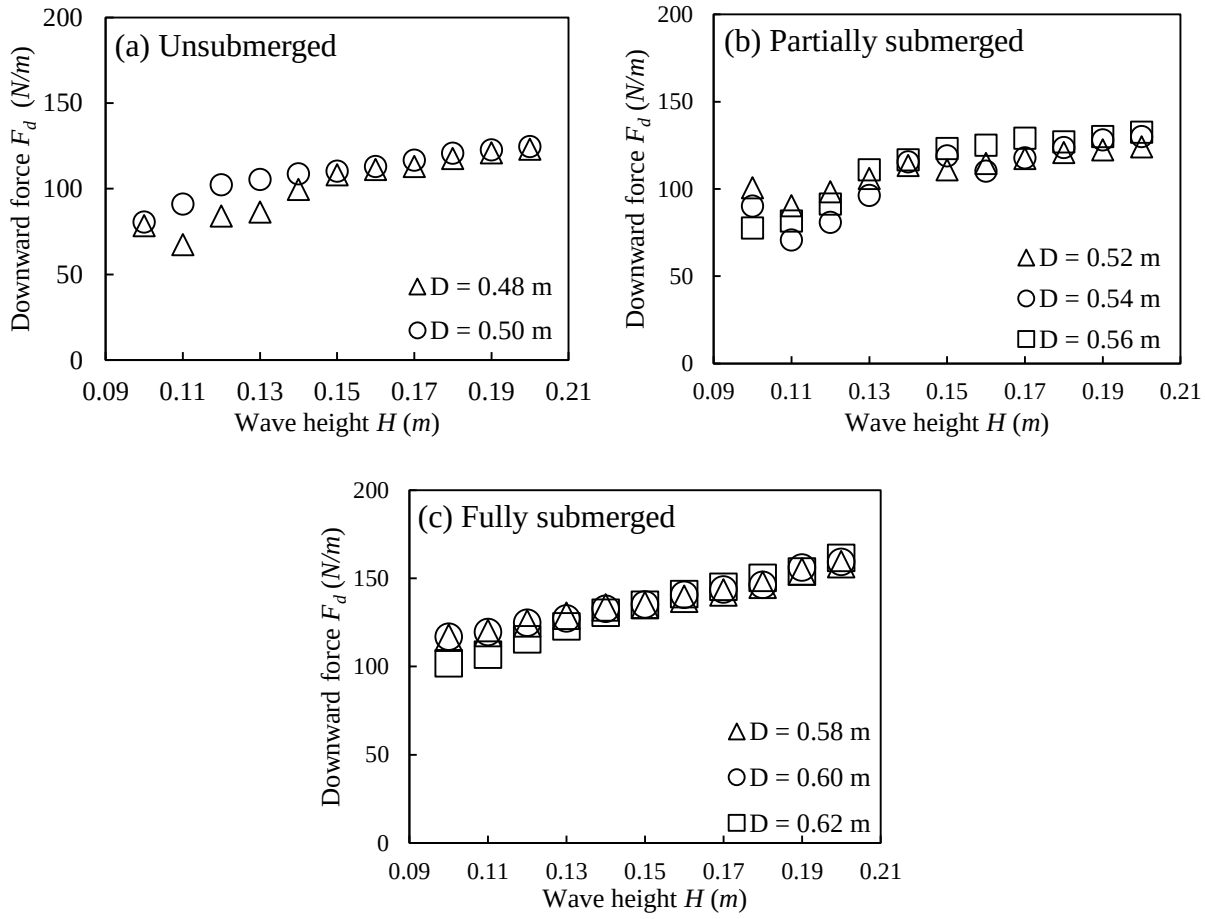

Fig. 13 Experimentally measured vertical downward wave forces for the deck with girders

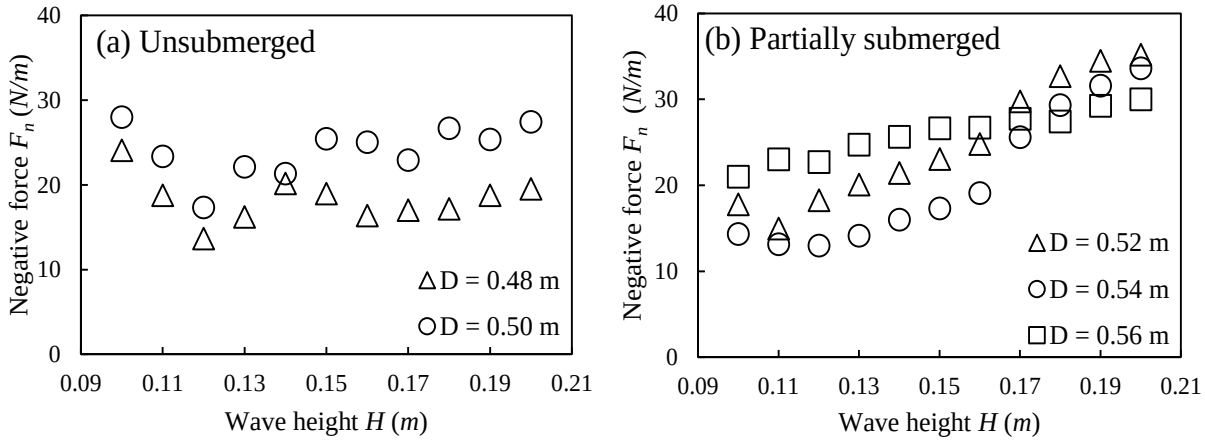

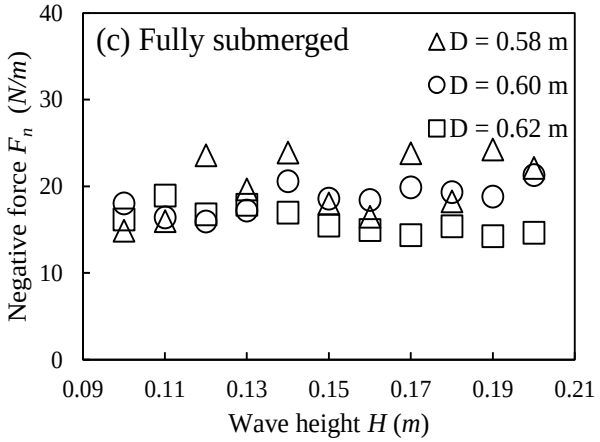

Fig. 14 Experimentally measured horizontal negative wave forces for the deck with girders

2.4. Analytic equation of maximum solitary wave force based on experimental data

In order to reduce the number and complexity of parameters, a dimensionless analysis is presented in this part with the ratio of wave height H to wavelength λ plotted along the x axis, and wave loads acting on unit length of the bridge model plotted along the y axis. Fig. 15 shows the dimensionless analysis for the no girders cases. It is obvious that for all the values of D, a good linear relationship can be found between uplift wave forces and wave steepness, which is the ratio of wave height H to wavelength λ. The wave steepness can also be derived from H and D based on generation wave theory discussed in section 2, as follows:

$$S = \frac{H}{\lambda} = 0.114\left(\frac{H}{D}\right)^{\frac{3}{2}} \tag{5}$$

Figs. 15(a) and 15(b) present the results for unsubmerged cases and partially or fully submerged cases for deck with girders cases, respectively. The linear relationship is well observed in all the experimental data. An analytical equation for the quantification of uplift wave force is proposed as:

$$F_u = a\gamma_s\gamma_r S + b = a\gamma_s\gamma_r\left(\frac{H}{D}\right)^{\frac{3}{2}} + b \tag{6}$$

where F_u is the uplift wave force; γ_s and γ_r are parameters accounting for dimensions of bridge superstructures and relative position of the bridge and SWL; and a and b are fitting coefficients.

Similar linear relationships can also be found with respect to the horizontal positive force F_p. Therefore, wave steepness S might be adopted as an important parameter in calculating solitary wave loads. Most of previous research tried to establish the relationship among F_u, H and D at the same time, but seldom reached a good result. By introducing steepness S, the wave-induced force can be estimated more concisely and precisely.

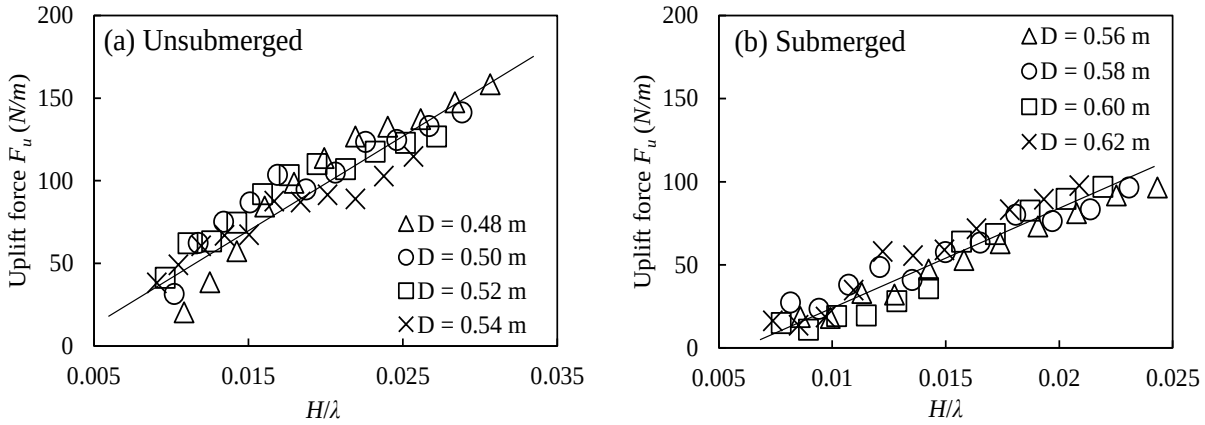

Fig. 15 Relationship between the uplift force and wave steepness for deck without girders

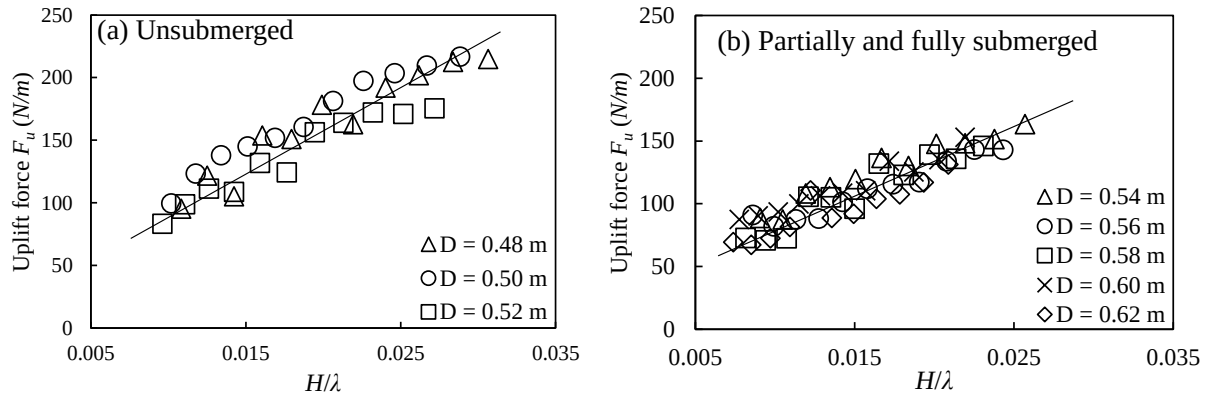

Fig. 16 Relationship between uplift force and wave steepness for deck with girders

3. Numerical investigation

In addition to the experiments, the numerical studies are also conducted in this paper. By comparing the results from experiments and numerical calculation, the numerical methodology could be verified. Then, variable scales and scenarios can be assessed. In this section, the general concept and governing equation of Computational Fluid Dynamics (CFD) are introduced. All the cases are calculated using the commercial software *ANSYS Fluent* (v.17.2) to solve the

fundamental partial differential Navier-Stokes equations, which has been proven effective in previous research (Hamza *et al.* 2015; Xu *et al.* 2016b; Xu *et al.* 2017a). Model setup and boundary conditions for both 2D and 3D models are presented as well. To better capture the turbulent fluctuations of bridge deck-wave interactions, the shear-stress transport (SST k-ω) model is used as the turbulence closure for the Reynolds-averaged Navier-Stokes (RANS) equations (Menter 1994).

For the setups of the SST k-ω model in *ANSYS Fluent*, the pressure-based solver (segregated) is chosen for the transient flow, which is good at resolving incompressible fluid motion. For the velocity inlet boundary, outlet boundary, and top boundary, the turbulence intensity and turbulent viscosity ratio are set as 2% and 10%, respectively. The Pressure-Implicit with Splitting of Operators scheme (PISO) is used for the pressure-velocity coupling method (Bricker *et al*. 2011, 2014), and the PREssure STaggering Option (PRESTO) scheme is utilized for pressure spatial discretization due to its good performance dealing with irregular complex interface of the structure model. Least squares cell-based scheme is used for the gradient discretization. The second order upwind is utilized for calculating the momentum, volume fraction, turbulent kinetic energy, and specific dissipation rate (Murillo 2008). Such second order upwind also has good convergence during the calculation process.

The volume of fluid (VOF) method is used to determine the dynamic free surface (Hirt and Nichols 1981). As for the numerical model input, the water particle velocity components u and v, water pressure p and the free surface profile η are (Sarpkaya and Isaacson 1981):

Similarly, the solitary wave crest is located at $x = 0$ when $t = 0$ s, which is just at the velocity inlet boundary. Thus, in order to more accurately simulate the wave profile, the solitary wave should be shifted leftward by utilizing a coefficient t_0 to adjust t. In this way, the water surface can increase gradually at the inlet boundary and a fully developed solitary wave profile can be generated. The equations of wave velocity particles u and v are interpreted into *Fluent* by using User Defined Functions (UDF).

3.1. Numerical model set-up

To ensure the efficiency and accuracy of the numerical model, a mesh sensitivity study is conducted. Different mesh resolutions including dx = 0.005 m, 0.004 m and 0.003 m in the x

direction and dz = 0.005 m, 0.004 m and 0.003 m in the z direction. The obtained results show that there are no significant differences on the achieved wave profiles. Therefore, the cell dimensions are determined as dx = 0.005 m and dz = 0.005 m. The fixed time step dt = 0.002 s is adopted to satisfy the requirement of the Courant Number. A small dt may also affect the accuracy of calculating vertical wave force (Bozorgnia and Lee 2012). In order to save the computation time, especially for 3D model, meshes for the top air zone, deep water zone, and near outlet zone are relatively coarsen.

Fig. 17(a) shows the schematic diagram of the 2D numerical domain of the 1:30 bridge model. The total numerical domain is 1.5 m in height and 10 m in length, which is long enough to eliminate wave reflection effect. Line CD is the SWL, separating the interface of air and water; line AB is set as pressure outlet with the constant atmosphere pressure (i.e., 101,325 Pa); line AE is the velocity inlet, with input velocity controlled by the user-defined function; line EF is the no-slip stationary wall condition; and line BF acts as the pressure outlet to keep the balanced pressures for the air and water zones.

Fig. 17(b) shows the 3D numerical model of the deck with girders. Compared with the 2D model, in order to reduce the number of total grids and calculation time, a symmetry plane is used in the middle of the model. Plane ABDC is the velocity inlet, where solitary waves are generated using the UDF functions, same as the 2D numerical method. Plane EFHG is the pressure outlet to keep a free water surface level at the end of water flow and reduce the influence of wave reflections. Plane ABFE is set as the pressure outlet to apply a constant atmosphere pressure of 101.325 kPa. Plane CDHG and BDHF are no-slip walls to simulate the bottom and the side of the tank respectively. Plane ACGE is the symmetry plane to speed up the calculation. The superstructure model is also half of the original model and set at the symmetry plane. Other parameters are similar with the 2D numerical model.

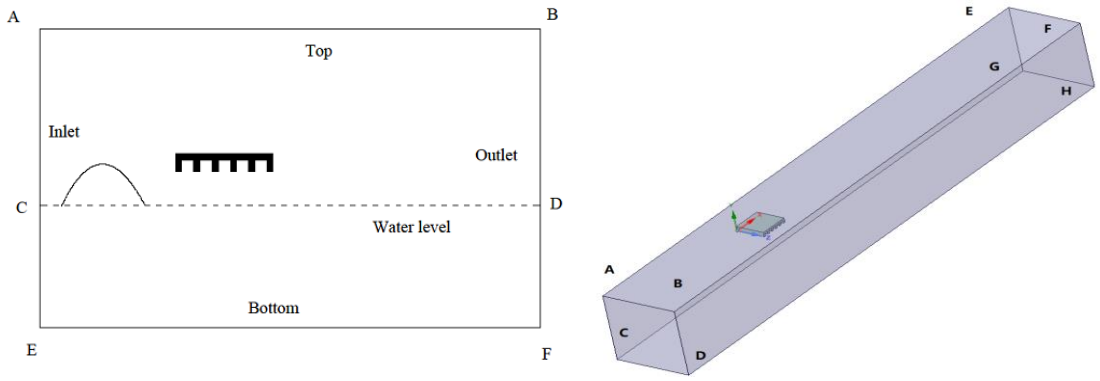

Fig. 17 (a) 2D and (b) 3D numerical models

3.2. Model validation

To verify the accuracy of the numerical model, a comparison of time series of the computed solitary wave generated by *ANSYS Fluent* with the laboratory measurements is shown in Fig. 18. Positions of three wave gauges and bridge model are shown in Fig. 18(a). The initial water depth is set as 0.5 *m* and the expected wave height is 0.15 *m*. Due to different setting positions and slight friction resistance caused by the sidewall of wave channel, the readings of these three wave gauges and the time to peak are slightly different. Numerical results are also presented in Fig. 18(b). As indicted, little but reasonable differences are observed.

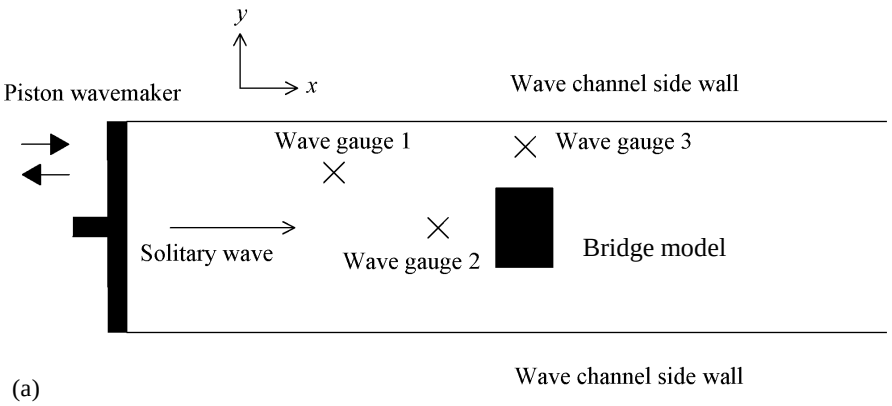

(a)

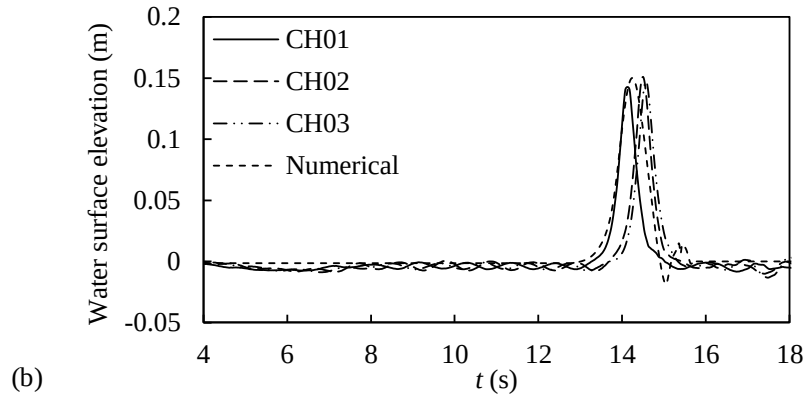

Fig. 18 (a) Top view of setups and positions of wave gauges and (b) comparison of simulated solitary wave with experimental results

4. Comparison between numerical results and experimental data

In this section, several cases are chosen for detailed comparison between experimental data and numerical analysis. The performance of 2D and 3D models, the effect of girders and trapped air, and the causes of the secondary impact are discussed.

4.1. Comparison of peak forces

Computations are performed for all the experimental cases. In this section, the result for one typical case, $D = 0.50\ m$, is presented for illustrative purpose. As indicated in Fig. 19, both numerical and measured results for deck with and without girders are presented. Overall, good agreement between the computations and measurements is observed in both cases. For the unsubmerged and partially submerged cases, that is $H < 0.15\ m$, the agreement is better for both models, but obvious deviations occur for the deck with girders after H reaches $0.15\ m$, while the no girders cases still match well. In general, the 2D model would reveal larger uplift forces for the girder deck under all the wave heights.

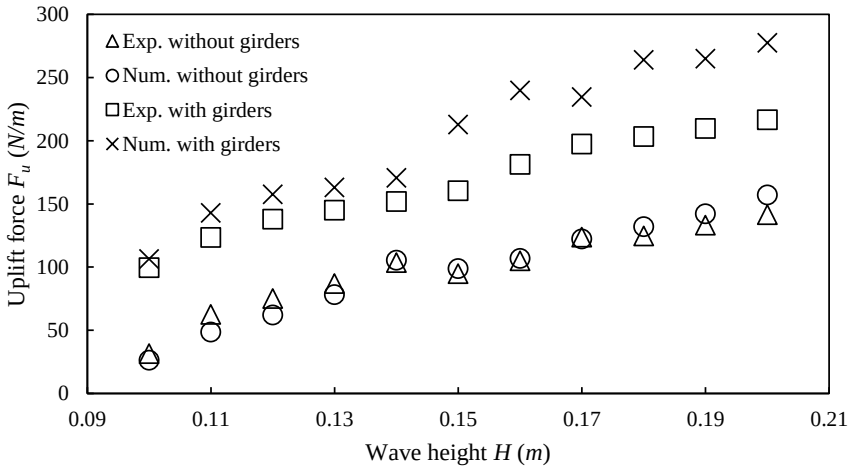

Fig. 19 Comparison between 2D numerical analysis and experimental results

4.2. Comparison of force time histories

In order to have a better understand in the differences between numerical analysis and experiments, a comparison of wave force time history for the deck with girders is shown in Fig. 20. Both computational models match the experimental data well, but the 3D model provides an improvement over the 2D model. The 3D model captures the vertical forces very well, improving upon the estimation of the 2D model both at more precise peak value and the secondary impact. For the 2D model, it fails to account for the complicated wave-deck interaction caused by irregular contact shape, forced area, and trapped air. The 2D model cannot simulate the air discharge in transverse direction before the wave crest arrives and overestimates uplift force caused by compressed air between girders. Generally, the 2D model is adequate to reproduce simple wave flume experiments, in which the structural dimension is simple and regular, and provides conservative calculation results. For a complex structure, such as irregular shapes with girders, bridge deck with combination of skew and slope, or a bridge spanning with non-uniformities, results with 2D model may be inaccurate or impractical. The 3D model should be adopted for these cases to achieve more accurate results.

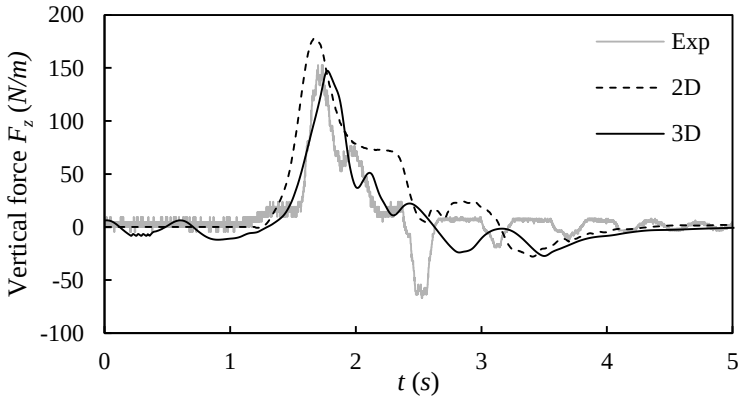

Fig. 20 Comparison of time histories of vertical wave forces for the deck with girders given D = 0.48 m and H = 0.13m

4.3. Comparison of wave profiles

The wave profiles during the wave-structure interaction from the 2D model, 3D model, and experiment for the same case with wave height $H = 0.15\ m$ are demonstrated in Fig. 21. The solitary wave comes from the right side to the left in these figures. In the numerical cross-sectional domain, the blue represents air, red represents water, and other colors in between represent the mixture of water and air according to the VOF method.

When the solitary wave approaches and first exceeds the top of deck, overtopping occurs, water splashes, and waveshape deforms. This could result in the first impact on the bridge deck. Then, after the first impact, the wave keeps moving forward with splashes, resulting in mixed fluid phases around the deck. During this phase, as the water level gradually rises, the air between the water and the bridge is first trapped, and then squeezed out from both the wave direction and the gaps between the girders (in x and y directions). The bubbles are observed during the experimental studies as indicted in Fig. 21(c). The partial release of trapped air may cause structural unequilibrium as well as the secondary impact measured in force time histories.

The trapped air between the deck and girders is simulated in the 2D model, but the 2D model fails to capture the dynamic air escape process due to the model limitation in z direction. Under this condition, the trapped air could cause an overestimation of the total forces, which agrees with the results of previous study (Xu *et al.* 2017b). The 3D model successfully simulates the water-air interaction owing to its spatial scalability and it could simulate the mixture of these two phases beneath the deck. Therefore, the 3D model could provide more information on the calculation of

peak force and better capture the force time series and the secondary impact. Such feature further indicates that the partial release of trapped air could contribute to the secondary impact force.

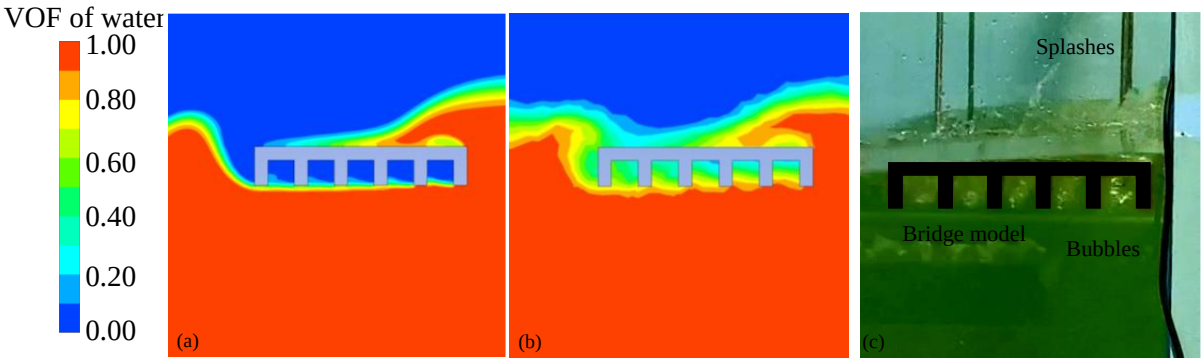

Fig. 21 Wave profiles from (a) 2D numerical model; (b) 3D numerical model; and (c) experiment

5. Conclusions

This study focuses on the experimental and numerical analysis of solitary waves effects on bridge superstructure. Specifically, the experiment of the wave force on bridge superstructure was performed at the hydraulics laboratory and numerical analysis based on 2D model and 3D model were conducted to have a comparison on their performance in simulating this process. Both bridge deck model with and without girders were tested to further assess the effects of girders and trapped air. An analytical equation is proposed to compute the wave-inducted force by incorporating the wave steepness parameter.

The results from the series of investigations show that for the deck without girders model in unsubmerged cases, vertical uplift forces and horizontal positive forces are approximately proportional to wave height, but decrease with larger initial water depth. Vertical downward forces and horizontal negative forces tend to decrease first and then increase as the wave height increases for most of the unsubmerged cases. For submerged cases, all these four forces have a near-linear relationship with the wave height. For the deck with girders group, the vertical uplift forces increase with wave heights in the unsubmerged, partially submerged and fully submerged cases. They increase fastest in unsubmerged cases and slowest in fully submerged cases. As indicated, the influence of wave height is much more obvious in shallow water. Similar trend can be observed for horizontal positive forces as well. Vertical uplift forces and positive horizontal forces are

relatively smaller when the wave crest has little or no interaction with the bridge deck. Maximum values are observed when the wave crest has a similar height of the bridge. It can be concluded that such interaction contributes significantly to force magnitude.

A secondary impact which may be caused by the trapped air is observed associated with the case of deck with girders. In addition, after conducting the dimensionless analysis, we found a linear relationship between wave forces and wave steepness by using measured experimental data. According to the used solitary wave theory and wave generation method, and substituting measured results, a load calculation formula for solitary waves acting on bridge superstructure is quantified.

As for the numerical analysis, the comparison between 2D numerical analysis and experiments shows good agreement for most cases, except for some cases where trapped and compressed air may play an important role. The 3D model captures the wave forces better, improving upon the estimation of the peak value and secondary impulse compared with 2D model. In addition, the flow and escape of the trapped air is better simulated in the 3D model, providing a more reliable result. For a complex structure, such as irregular shapes with girders, bridge deck with combination of skew and slope, or a bridge spanning with non-uniform cross-section, the 3D model should be adopted to assess the peak value and the whole loading process.

From the measurements, calculations and comparisons of all the data, the following conclusions and suggestions are made:

1. Solitary wave forces on bridge decks consist of uplift and positive forces. For the investigated cases, the uplift forces are larger than downward and negative forces.
2. For the experimental model, the existence of girders increases total wave loads on the superstructure. The bluff profile also leads to severe wave-deck interaction and structure vibration. Dynamic response analysis of bridge under extreme conditions is necessary.
3. A secondary impact after the first peak associated with the wave force is observed, which may be caused by the release of the trapped air between girders beneath the deck. Such impulse may occur with a large overturning moment simultaneously and may cause damage and failure to the bridges.
4. The secondary impact force may be caused by the release of trapped air between girders, and it becomes smaller for larger initial water depth with less trapped air, but not as much

as the maximum force decreases. As the initial water surface rises, the maximum force decreases significantly, while the secondary peak changes little. The maximum uplift force is almost twice of the second peak in unsubmerged case, but they are almost the same in the partially submerged case and fully submerged case.

5. Solitary wave loads can be assumed to be proportional to the wave steepness, and the relevant coefficients can then be determined based on structural parameters.
6. Wave steepness deserves more attention in calculating tsunami and hurricane wave loads. For example, it can be used as an intensity measure for the structural performance assessment.
7. The 3D model has a superior performance in simulating the water-gas interaction during the wave process and provides more accurate results. With an improved 3D model, it is possible to deal with bridges with slopes and curves.

In general, future related research should carefully consider the following aspects: dynamic response analysis considering the bridge substructure and the connection between the superstructure and substructure; 3D model numerical analysis to further investigate the trapped air effects and to quantify the total loads; and a coupled fluid-structure-interaction model (in 2D or 3D) to reproduce the process.

Acknowledgment

The study has been supported by The Hong Kong Polytechnic University under Start-Up Fund number 1-ZE7Q and the Research Grant Council of Hong Kong (ECS project No. PolyU 252161/18E). The opinions and conclusions presented in this paper are those of the authors and do not necessarily reflect the views of the sponsoring organizations.

References

Akiyama, M., Frangopol, D. M., Arai, M., & Koshimura, S. (2012). Probabilistic assessment of structural performance of bridges under tsunami hazard. In *Structures Congress 2012American Society of Civil Engineers*.

ANSYS®, Release 17.2, Fluent Theory Guide, ANSYS, Inc.

Ataei, N., & Padgett, J. E. (2012). Probabilistic modeling of bridge deck unseating during hurricane events. *Journal of Bridge Engineering*, *18*(4), 275-286.

Azadbakht, M., & Yim, S. C. (2016). Effect of trapped air on wave forces on coastal bridge superstructures. *Journal of Ocean Engineering and Marine Energy*, *2*(2), 139-158.

Biésel, F., & Suquet, F. (1951). Les appareils générateurs de houle en laboratoire. *La houille blanche*, (2), 147-165.

Boccotti, P. (1995). A field experiment on the small-scale model of a gravity offshore platform. *Ocean engineering*, *22*(6), 615-627.

Boussinesq, J. (1872). Théorie des ondes et des remous qui se propagent le long d'un canal rectangulaire horizontal, en communiquant au liquide contenu dans ce canal des vitesses sensiblement pareilles de la surface au fond. *Journal de mathématiques pures et appliquées*, 55-108.

Bozorgnia, M., & Lee, J. J. (2012). Computational fluid dynamic analysis of highway bridges exposed to hurricane waves. *Coastal Engineering Proceedings*, *1*(33), 70.

Bradner, C., Schumacher, T., Cox, D., & Higgins, C. (2011). Large–Scale Laboratory Observations of Wave Forces on a Highway Bridge Superstructure.

Bricker, J. D., Kawashima, K., & Nakayama, A. (2011). CFD analysis of bridge deck failure due to tsunami. In *Proceedings of the international symposium on engineering lessons learned from the* (pp. 1-4).

Bricker, J. D., & Nakayama, A. (2014). Contribution of trapped air, deck superelevation, and nearby structures to bridge deck failure during a tsunami. *Journal of hydraulic engineering*, *140*(5), 05014002.

Chen, Q., Kirby, J. T., Dalrymple, R. A., Kennedy, A. B., & Chawla, A. (2000). Boussinesq modeling of wave transformation, breaking, and runup. II: 2D. *Journal of Waterway, Port, Coastal, and Ocean Engineering*, *126*(1), 48-56.

Crowley, R., Robeck, C., & Dompe, P. (2018). A three-dimensional computational analysis of bridges subjected to monochromatic wave attack. *Journal of Fluids and Structures*, *79*, 76-93.

Cuomo, G., Shimosako, K. I., & Takahashi, S. (2009). Wave-in-deck loads on coastal bridges and the role of air. *Coastal Engineering*, *56*(8), 793-809.

Dong, Y., & Frangopol, D.M. (2017). Adaptation optimization of residential buildings under hurricane threat considering climate change in a life-cycle context. *Journal of Performance of Constructed Facilities*, 31(6), 04017099, 1-10.

Douglass, S. L., Hughes, S., Rogers, S., & Chen, Q. (2004). The impact of Hurricane Ivan on the coastal roads of Florida and Alabama: a preliminary report. *Rep. to Coastal Transportation Engineering Research and Education Center, Univ. of South Alabama, Mobile, Ala*.

Fang, Q., Hong, R., Guo, A., & Li, H. (2019a). Experimental Investigation of Wave Forces on Coastal Bridge Decks Subjected to Oblique Wave Attack. *Journal of Bridge Engineering*, *24*(4), 04019011.

Fang, Q., Yang, C., & Guo, A. (2019b). Hydrodynamic Performance of Submerged Plates During Focused Waves. *Journal of Marine Science and Engineering*, *7*(11), 389.

Frangopol, D.M., Dong, Y., & Sabatino, S. (2017). Bridge life-cycle performance and cost: Analysis, prediction, optimization and decision making. *Structure and Infrastructure Engineering*, 13(10), 1239-1257.

French, J. A. (1970). *Wave uplift pressures on horizontal platforms* (Doctoral dissertation, California Institute of Technology).

Goring, D. G. (1978). Tsunamis--the propagation of long waves onto a shelf.

Guo, A., Fang, Q., Bai, X., & Li, H. (2015a). Hydrodynamic experiment of the wave force acting on the superstructures of coastal bridges. *Journal of Bridge Engineering*, *20*(12), 04015012.

Guo, A., Fang, Q., & Li, H. (2015b). Analytical solution of hurricane wave forces acting on submerged bridge decks. *Ocean Engineering*, *108*, 519-528.

Guo, A., Liu, J., Chen, W., Bai, X., Liu, G., Liu, T., ... & Li, H. (2016). Experimental study on the dynamic responses of a freestanding bridge tower subjected to coupled actions of wind and wave loads. *Journal of Wind Engineering and Industrial Aerodynamics*, *159*, 36-47.

Hamza, S. B., Habli, S., Saïd, N. M., Bournot, H., & Le Palec, G. (2015). Numerical simulation of wave-structure interaction around an obstacle. In *Design and Modeling of Mechanical Systems-II* (pp. 683-691). Springer, Cham.

Hayatdavoodi, M., & Ertekin, R. C. (2016). Review of wave loads on coastal bridge decks. *Applied Mechanics Reviews*, *68*(3), 030802.

Hayatdavoodi, M., Seiffert, B., & Ertekin, R. C. (2014). Experiments and computations of solitary-wave forces on a coastal-bridge deck. Part II: Deck with girders. *Coastal Engineering*, *88*, 210-228.

Hirt, C. W., & Nichols, B. D. (1981). Volume of fluid (VOF) method for the dynamics of free boundaries. *Journal of computational physics*, *39*(1), 201-225.

Huang, B., Duan, L., Yang, Z., Zhang, J., Kang, A., & Zhu, B. (2019a). Tsunami Forces on a Coastal Bridge Deck with a Box Girder. *Journal of Bridge Engineering*, *24*(9), 04019091.

Huang, B., Yang, Z., Zhu, B., Zhang, J., Kang, A., & Pan, L. (2019b). Vulnerability assessment of coastal bridge superstructure with box girder under solitary wave forces through experimental study. *Ocean Engineering*, *189*, 106337.

Huang, W., & Xiao, H. (2009). Numerical modeling of dynamic wave force acting on Escambia Bay Bridge deck during Hurricane Ivan. *Journal of Waterway, Port, Coastal, and Ocean Engineering*, *135*(4), 164-175.

Huseby, M., & Grue, J. (2000). An experimental investigation of higher-harmonic wave forces on a vertical cylinder. *Journal of Fluid Mechanics*, *414*, 75-103.

James, D., Cleary, J., & Douglass, S. (2015). Estimating wave loads on bridge decks. In *Structures Congress 2015American Society of Civil Engineers*.

Jin, J., & Meng, B. (2011). Computation of wave loads on the superstructures of coastal highway bridges. *Ocean Engineering*, *38*(17-18), 2185-2200.

Kennedy, A. B., Chen, Q., Kirby, J. T., & Dalrymple, R. A. (2000). Boussinesq modeling of wave transformation, breaking, and runup. I: 1D. *Journal of waterway, port, coastal, and ocean engineering*, *126*(1), 39-47.

Kosa, K. (2011). Damage analysis of bridges affected by tsunami due to Great East Japan Earthquake. In *Proceedings of the International Symposium on Engineering Lessons Learned from the* (pp. 1-4).

Laitone, E. (1963). *Higher order approximation to nonlinear waves and the limiting heights of cnoidal, solitary and stokes waves. Beach Erosion Board, US Department of the Army, Corps of Engineers* (No. 133). Technical Memorandum.

Lee, J. J., & Lai, C. P. (1987). Wave uplift on platforms or docks in variable depth. In *Coastal Engineering 1986* (pp. 2023-2034).

McCowan, J. (1891). VII. On the solitary wave. *The London, Edinburgh, and Dublin Philosophical Magazine and Journal of Science*, *32*(194), 45-58.

McPherson, R. L. (2008). Hurricane induced wave and surge forces on bridge decks. *A Thesis, Texas A&M University*.

Menter, F. R. (1994). Two-equation eddy-viscosity turbulence models for engineering applications. *AIAA journal*, *32*(8), 1598-1605.

Motley, M. R., Wong, H. K., Qin, X., Winter, A. O., & Eberhard, M. O. (2015). Tsunami-induced forces on skewed bridges. *Journal of Waterway, Port, Coastal, and Ocean Engineering*, *142*(3), 04015025.

Murillo, J., García‐Navarro, P., & Burguete, J. (2008). Analysis of a second‐order upwind method for the simulation of solute transport in 2D shallow water flow. *International journal for numerical methods in fluids*, *56*(6), 661-686.

Naheer, E. (1977). Stability of bottom armoring under the attack of solitary waves.

Okeil, A. M., & Cai, C. S. (2008). Survey of short-and medium-span bridge damage induced by Hurricane Katrina. *Journal of Bridge Engineering*, *13*(4), 377-387.

Padgett, J., DesRoches, R., Nielson, B., Yashinsky, M., Kwon, O. S., Burdette, N., & Tavera, E. (2008). Bridge damage and repair costs from Hurricane Katrina. *Journal of Bridge Engineering*, *13*(1), 6-14.

Robertson, I. N., Riggs, H. R., Yim, S. C., & Young, Y. L. (2007a). Lessons from Hurricane Katrina storm surge on bridges and buildings. *Journal of Waterway, Port, Coastal, and Ocean Engineering*, *133*(6), 463-483.

Robertson, I. N., Yim, S., Riggs, H. R., & Young, Y. L. (2007b). Coastal bridge performance during Hurricane Katrina. In *Third International Conference on Structural Engineering, Mechanics and Computation, SEMC-2007, Cape Town, South Africa, Millpress, Rotterdam, The Netherlands* (pp. 1864-1870).

Sarpkaya, T., & Isaacson, M. (1981). Mechanics of wave forces on offshore structures.

Schäffer, H. A. (2002). Active wave absorption in flumes and 3D basins. In *Ocean Wave Measurement and Analysis (2001)*(pp. 1200-1208).

Seiffert, B. R. (2014). *Tsunami and storm wave impacts on coastal bridges* (Doctoral dissertation, [Honolulu]:[University of Hawaii at Manoa],[December 2014]).

Seiffert, B., Ertekin, R. C., & Robertson, I. N. (2014a). Experimental investigation on the role of entrapped air on solitary wave forces on a coastal bridge deck. In *ASME 2014 33rd International Conference on Ocean, Offshore and Arctic Engineering* (pp. V04BT02A039-V04BT02A039). American Society of Mechanical Engineers.

Seiffert, B. R., Ertekin, R. C., & Robertson, I. N. (2015). Wave loads on a coastal bridge deck and the role of entrapped air. *Applied Ocean Research*, *53*, 91-106.

Seiffert, B., Hayatdavoodi, M., & Ertekin, R. C. (2014b). Experiments and computations of solitary-wave forces on a coastal-bridge deck. Part I: Flat plate. *Coastal Engineering*, *88*, 194-209.

Xiao, H., Huang, W., & Chen, Q. (2010). Effects of submersion depth on wave uplift force acting on Biloxi Bay Bridge decks during Hurricane Katrina. *Computers & Fluids*, *39*(8), 1390-1400.

Xu, G., Cai, C. S., & Chen, Q. (2016a). Countermeasure of air venting holes in the bridge deck–wave interaction under solitary waves. *Journal of Performance of Constructed Facilities*, *31*(1), 04016071.

Xu, G., Cai, C. S., Hu, P., & Dong, Z. (2016b). Component level–based assessment of the solitary wave forces on a typical coastal bridge deck and the countermeasure of air venting holes. *Practice Periodical on Structural Design and Construction*, *21*(4), 04016012.

Xu, G., Chen, Q., Zhu, L., & Chakrabarti, A. (2017a). Characteristics of the wave loads on coastal low-lying twin-deck bridges. *Journal of Performance of Constructed Facilities*, *32*(1), 04017132.

Xu, G., Cai, C., & Deng, L. (2017b). Numerical prediction of solitary wave forces on a typical coastal bridge deck with girders. *Structure and Infrastructure Engineering*, *13*(2), 254-272.